Hierarchical Structured Multifunctional Self-Cleaning Material with Durable Superhydrophobicity and Photocatalytic Functionalities

Zhang, Xiaotian ; Liu, Shanqiu ; Salim, Alma ; Seeger, Stefan

Abstract: Self-cleaning materials, which are inspired and derived from natural phenomena, have gained significant scientific and commercial interest in the past decades as they are energy- and labor-saving and environmentally friendly. Several technologies are developed to obtain self-cleaning materials. The combination of superhydrophobic and photocatalytic properties enables the efficient removal of solid particles and organic contaminations, which could reduce or damage the superhydrophobicity. However, the fragility of the nanoscale roughness of the superhydrophobic surface limits its practical application. Here, a hierarchical structure approach combining micro- and nanoscale architectures is created to protect the nanoscale surface roughness from mechanical damage. Glass beads of 75 mu m are partially embedded into a low-density polyethylene film. This composite surface is coated with silicone nanofilaments (SNFs) via the droplet-assisted growth and shaping approach, providing the nanoscale surface roughness as well as the support for the photocatalyst with enlarged surface area. TiO2 nanoparticles, which serve as the photocatalyst, are synthesized in situ on SNFs through a hydrothermal reaction. The self-cleaning effect is proved using wettability measurements for various liquids, degradation of organic contamination under UV light, and antibacterial tests. The enhanced mechanical durability of the hierarchical structure of the composite material is verified with an abrasion test.

DOI: https://doi.org/10.1002/smll.201901822

Hierarchical Structured Multi-functional Self-cleaning Material with Durable Superhydrophobicity and Photocatalytic Functionalities

*Xiaotian Zhang[#], Shanqiu Liu[#], Alma Salim, Stefan Seeger**

[#]These authors contributed equally to this study

Xiaotian Zhang[#], Dr. Shanqiu Liu[#], Alma Salim, Prof. Dr. Stefan Seeger

Department of Chemistry, University of Zurich, Winterthurerstrasse 190, 8057 Zurich, Switzerland

E-mail: sseeger@chem.uzh.ch

Keywords: self-cleaning, superhydrophobic, photocatalytic, hierarchical structure, mechanical durable

Abstract:

Self-cleaning materials, which are inspired and derived from natural phenomena like the surface structures of the lotus leaf and butterfly wings, have gained significant scientific and commercial interest in the past decades since they are energy- and labour-saving and environmentally friendly. Several technologies have been developed to obtain self-cleaning materials. Among them, the combination of superhydrophobic and photocatalytic properties enables the efficient removal of solid particles and organic contaminations, which could reduce or even damage the superhydrophobicity. However, the fragility of the nanoscale roughness of the superhydrophobic surface limits its practical application. Here, a hierarchical structure approach combining micro- and nanoscale architectures is created to protect the nanoscale surface roughness from mechanical damage. Briefly, 75-µm glass beads were partially embedded into a low-density polyethylene film. This composite surface is coated with silicone nanofilaments (SNFs) via the droplet-assisted growth and shaping approach, providing the nanoscale surface roughness as well as the support for the photocatalyst with enlarged surface area. TiO_2 nanoparticles, which serve as the photocatalyst, are synthesized in situ on SNFs through a hydrothermal reaction. The self-cleaning effect is proved using wettability

measurements for various liquids, degradation of organic contamination under UV light, and antibacterial tests. The enhanced mechanical durability of the hierarchical structure of the composite material is verified with an abrasion test.

1. Introduction

Self-cleaning materials inspired by nature, for example, the lotus leaf,[1] the legs of the water strider,[2] and the wings of cicada, [3] have attracted much attention due to their broad range of potential applications.[4] Some firms have attempted to commercialize the technology into labor-saving materials in multifunctional products used frequently in daily life.[5] In terms of the surface wettability, self-cleaning surfaces can be classified into two main categories, superhydrophilic and superhydrophobic. These two types lead to cleaning of the surface by different behaviors towards the water. Superhydrophilic surfaces, where the water contact angle is less than 5°, can be cleaned by the spreading of water across the surface or a stream of water, like rainfall.[6] In contrast, on superhydrophobic surfaces, water forms spherical droplets that roll across the surface, carrying away contamination particles.[7] This phenomenon is known as the “lotus effect”,[8] whose origin is the surface energy and the roughness of the corresponding surface.[9] In comparison, there are more advantages in choosing superhydrophobicity over superhydrophilictiy as self-cleaning materials due to the reduction of bacterial and contamination adhesion,[10] and their water-proof and anti-mist characteristics.[11] To achieve a superhydrophobic surface with a water contact angle of more than 150º, a low surface energy material is necessary, as well as a high roughness of micro- or nano-structured surface architecture. Therefore, hydrophobic polymers, alkyl silanes, or semi-fluorinated silanes are candidates for the generation of superhydrophobic surfaces.[12] Methods for constructing nano- or microstructure surfaces are important for realizing superhydrophobic surfaces. However, these methods are limited to particular substrates (*e.g.*, silicon wafer or aluminum foil) or by

the complexity of processing (*e.g.*, lithography and anodization), which restrict its broader applications. Moreover, surface superhydrophobicity could be damaged by the oily contamination from organic compounds or bacterial biofilm.[13] Thus a functionality which can maintain the surface superhydrophobicity is of pivotal importance to keep the durability of self-cleaning materials. One of the most convenient and effective ways to achieve that is through compositing photocatalysts.

Artificial photocatalytic surfaces have become increasingly popular over the recent decades since their discovery by Fujishima and Honda in 1972.[14] Among photocatalytic materials, TiO_2 has attracted much attention in scientific research as well as commercial applications. TiO_2 is well-known as an efficient photocatalyst in air and water purification, water splitting, and the disinfection of surfaces.[15] It has been demonstrated that including TiO_2 in the composition of a surface coating is a good approach to fabricating self-cleaning materials.[16] In addition to the photocatalytic properties, one of the most reported features of TiO_2 is the superhydrophilicity of the surface. Low water contact angles (less than 10º) were observed at different amounts of TiO_2 added.[17] If superhydrophobic surfaces are preferred for constructing self-cleaning materials, the modification of a TiO_2 containing surface is indispensable. For instance, Yamashita et al developed a co-deposition technique to generate a superhydrophobic and photocatalytic surface consisting TiO_2 and polytetrafluoroethylene.[18]However, this functional surface features poor mechanical durability as well as negative impacts on the environment due to the involved fluorides.

Silicone nanofilaments (SNFs) have been applied in various fields since their discovery in 2003,[19] including superhydrophobicity, superoleophobicity, photocatalysis, oil/water separation, and protein enrichment.[20] The superhydrophobicity of SNFs was achieved by the assembled 3D carpet surface morphology together with the low surface energy from silane precursors through a convenient vapor phase deposition on diverse substrates. Also, the feasibility of coating SNFs on different kinds of substrates makes them a broadly applicable

surface coating method.[21] Moreover, Nanostructured surfaces coated with SNFs enables a higher loading amount of photocatalysts due to their nanostructured morphology compared to the uncoated pristine surfaces, meanwhile the loaded photocatalysts can improve the resistance of surperhydrophobic surfaces against oily/biological contaminants.[22] Thus, the combination of SNFs and TiO_2 is very promising for strengthening the superhydrophobicity and photocatalysis of the surface as well as broadening the range of further applications.

However, the fragility of nano-dimensional protrusions (*e.g.*, SNFs) for generating the surface roughness according to the Cassie-Baxter model remains a challenge for creating a mechanical durable superhydrophobic surface.[23] A weak mechanical impact (*e.g.*, a finger wipe) on superhydrophobic surfaces leads to a loss of their non-wettability, resulting in the adhesion of water/contaminants on the substrate surface. Hierarchical roughness, which contains two or more length scales, increases the stability of the superhydrophobic surface structure.[24] The basic concept involves robust microscale structures providing spatial protection for relative fragile nanoscale protrusions (*e.g.*, SNFs) from mechanical damages, leading to the enhanced durability of the surface roughness and the non-wettability. For instance, hybrid porous micro/nanocomposites, textile fibers, protected SNFs composites, and hydrophobic coating sprayed wood are the typical applications based on the hierarchical roughness concept.[25]

Herein, we report a novel mechanical durable self-cleaning composite with superhydrophobic and photocatalytic degrading ability. Glass beads (75 μm in diameter) were drop cast on LDPE substrates, and partially embedded in the LDPE matrix by heating to 165°C, followed by coating of a homogeneous SNFs layer via droplet assisted growth and shaping (DAGS) method.[26] Through the hydrothermal reaction of TiF_4, TiO_2 nanoparticles were composited on SNFs.[27] Further hydrophobic treatment was performed to generate the final superhydrophobic substrate (**Figure 1**i). The novel composite exhibited excellent non-wettability showing a contact angle of 168° as well as a good photocatalytic ability for degrading the organic contaminants on the surface. Abrasion experiments proved that the material has mechanical

durability under certain pressure and the superhydrophobicity and photocatalytic properties could be well maintained after cyclic abrasion. In addition, the as-prepared composite material exhibited anti-bacterial properties and was verified to have great bacteria inhibition under UV illumination.

2. Results and Discussion

2.1. Preparation of the Functional LDPE Substrates

LDPE substrates were rinsed with ethanol and dried under nitrogen flow before use. A suspension of glass beads (GBs) in ethanol was treated with ultrasonication and constant magnetic stirring to avoid sedimentation. The suspension was drop cast on the LDPE substrate within a limited area (50 cm^2).[28] After evaporation of the ethanol from the surface, the substrate was baked in an oven at 165 °C for 10 min, followed by cooling to room temperature. The glass beads were embedded into the LDPE matrix with a defined depth.[29] The micrometer-sized structures, which can protect the nano-meter SNFs, were obtained as shown in **Figure 1**a. The embedding depth of the GBs was calculated by the diameter of the hole after the GBs were scratched off with a strong force (**Figure S**1), which was 20.82 µm.

Direct growth of SNFs on LDPE substrates was described in our previous work.[30] Here, we used a trifunctional silane $CH_3CH_2SiCl_3$ as a precursor. The growth conditions were optimized to produce a dense SNF coating with a high surface area that is suitable for further utility as a catalyst support (**Figure 1**b, c). The static contact angle of the obtained SNFs-GB-LDPE composite material was determined to be 165 ± 2°, with a sliding angle of 8 ± 1°. Though the micro-meter structured GBs were fixed on the substrate surface, the superhydrophobicity was in line with the findings of our previous studies (SNFs coated on a flat glass slide).[31] A side view of the SNFs-GB-LDPE substrates is presented in **Figure 1**e,f.

Subsequently, oxygen plasma treatment turned the surface completely hydrophilic with a contact angle of less than 10°, which proved that the surface was hydroxylated, benefiting the

next procedure of TiO_2 nanoparticles deposition. The well-dispersed TiO_2 NPs coating on SNFs was achieved by hydrothermal condensation of TiF_4 in ethanol/water at an elevated temperature. The reaction conditions were optimized based on a previous study in our group.[27] After 1 h of controlled hydrothermal reaction, TiO_2 NPs were deposited onto SNFs (**Figure 1**d). The SEM images show a homogeneous distribution of TiO_2 NPs with an average particle size from 40–100 nm all over the surface of SNFs. The particle size was further confirmed by TEM image in **Figure 1**g. However, the density of TiO_2 NPs observed in TEM image was lower compared with the one in the SEM image, which was due to the treatment of the sample by ultrasonication before TEM image acquisition.

The chemical composition was determined using energy dispersive X-ray analysis in STEM-EDX. The EDX spectra in **Figure 1**h shows that TiO_2 NPs were successfully immobilized on the SNFs. The silicon signal and part of the carbon and oxygen signals originated from SNF. The majority of the carbon signal and copper signal came from the formvar/carbon film-coated copper grid of the TEM sample holder. Titanium and part of the oxygen signals arise from TiO_2 NPs. Element analysis was also conducted by STEM EDX mapping of a single piece of functionalized SNF, as shown in **Figure 1**j.

In order to provide the TiO_2 deposited composite material with superhydrophobicity, the substrate was further hydrophobilized with the precursor (*i.e.*, ethyltrichlorosilane). In this procedure, the amount of precursor applied was 100 µL and the reaction time was limited to 20 min at 35% relative humidity. After the hydrophobic modification, the functional substrate was again switched from hydrophilic to superhydrophobic, with a slightly higher contact angle (168 ± 1°) and similar sliding angle (8.5±1.5°). Thus, a superhydrophobic functional LDPE matrix substrate with embedded GBs, coated with SNFs, and deposited TiO_2 NPs was achieved (illustrative graph in **Figure 1**i). Hereinafter the as-prepared superhydrophobic composite is referred to as TiO_2/SNFs-GBs-LDPE.

2.2. Self-cleaning Ability

With this new composite material, the self-cleaning property is expected to occur by two principal mechanisms: the superhydrophobicity of the surface was used to mechanically remove impurities by a water flow, with low adhesion on the surface; also, TiO_2 NPs are known to have photocatalytic activity and, therefore, catalyze the degradation of organic contaminants. In **Figure 2**a, a substrate is shown that was contaminated with µm/mm-sized chalk particles and drop cast methylene blue ethanol solution. Flushing with water leads to removal of the chalk particles (Video 1, 2 in supporting information). Rebounding of water was observed, proving the hydrophobicity of the substrate. We recorded the water repellence with a high-speed camera that clearly shows a rebound behavior of a 10-µL water drop (**Figure 2**b,c and video 3 in supporting information). The remaining organic contamination could not be rinsed off. However, it was decomposed and became invisible under UV illumination on the composite substrate. The comparison experiment result was shown in Supplemental **Figure S**2. Moreover, the surface was free of sticking of the various liquids (aqueous solutions or other liquids like Cola, red wine or milk) (**Figure 2**d).

To demonstrate the long-term stability, the contact angle was measured as a function of time under continuous UV irradiation (350 nm, 6.32 mW/cm^{-2}). As shown in Supplemental **Figure S3**a, the superhydrophobicity of the substrate did not change for 24 h. When exposed to the real environment under daily sunshine, the contact and sliding angles showed almost no change for 2 weeks. The slight drop of the contact angle might be due to the attachment of dust from the atmosphere (see Supplemental **Figure S3**b). Both experiments demonstrated the durability of the superhydrophobicity of the material.

When the substrate was contaminated by oleic acid in ethanol solution (3:7 v/v), the water contact angle dropped from 168° to 67°. Notably, after UV irradiation (light intensity: 6.32 mW/cm^{-2}), the water contact angle switches back to the original value. This is ascribed to the

induced TiO_2 NPs as the photocatalyst in our composite material. Free radicals are generated during the electron transfer induced by UV illumination, which leads to the photodegradation of oleic acid and the degradation products can be rinsed away with water.[32] After 20 cycles of oleic acid contamination and UV irradiation, the substrate remained stable for superhydrophobicity (**Figure 2**e) as well as morphology (**Figure S**4). Surface adhesion of the TiO_2/SNFs-GBs-LDPE composite after cyclic UV irradiation was characterized by the water sliding angle (SA) measurement as shown in **Figure S**5. After 20 cycles of UV irradiation, SA of the composite maintains around 10.5°.

The photocatalytic property of the functional substrate was demonstrated by the degradation test of methylene blue (MB) under UV illumination at 350 nm (intensity: 6.32 mW/cm^{-2}) in a methanol/water media (1:1 in volume in order to wet the material surface completely) with oxygen supply (30 mL/min) for 2 h. A Perkin-Elmer Lambda 650S, UV/vis spectrometer, was used to measure the absorbance from 350 nm to 900 nm, in which the absorbance peak shows the maximum at 665 nm. The light source – eight light bulbs (SNE Ultraviolet Co, USA) with emission wavelength at 350 nm – shows very little overlap compared with the absorption spectrum of MB (Supplemental **Figure S**6).

Figure 2f shows the absorption behavior of MB during degradation in the presence of solid substrates and the reference, respectively. There was only a small reduction of MB absorbance in the self-degradation (under UV illumination) without any photocatalytic substrates. After 2 h, the relative absorbance decreased by just 10.5%. To demonstrate the influence of SNFs on the loading amount of TiO_2 NPs and the consequent photocatalitic ability, a substrate without SNFs was treated with oxygen plasma, and subsequently, TiO_2 NPs were deposited (without prior growth of SNFs) according to the same hydrothermal method. The result shows that this sample reached a reduction of relative absorbance of MB of 23.4% after 120 min. The two substrates with TiO_2 NPs on SNFs: TiO_2/SNFs-LDPE (without the embedded GBs) and TiO_2/SNFs-GBs-LDPE, compared to these without growth of SNFs, achieved a much higher

photocatalytic activity resulting in a value of 88.9% and 89.3%, respectively. The result shows the exploiting of GBs on LDPE do not change the photocatalytic performance. It was concluded in our previous study that with additional surface roughness created by SNFs, the surface area of the substrate was much higher than the one without SNFs, multiplied by a factor of ca. 13.[33] Thus, this resulted in a correspondingly higher loading amount of TiO_2 NPs on the functional substrate, which significantly lowered the MB absorbance after UV irradiation. For further confirmation of the loading amount of TiO_2 NPs, the titanium content was determined by absorbance spectrometry at a wavelength of 410 nm. Substrates were immersed into highly concentrated sulfuric acid at 110°C for 30 min to dissolve all TiO_2 NP. The solution was then diluted 10-fold for measurement. The standard absorbance against concentration was calibrated with a standard solution before taking the measurement. The substrate without SNFs had a much less loading amount of TiO_2 NPs (about 0.183 mg/cm^2) relative to the functional substrates with SNFs of 1.85 mg/cm^2 for TiO_2/SNFs-GBs-LDPE and 1.87 mg/cm^2 for TiO_2/SNFs-LDPE due to the extended surface area provided by the SNFs.

The functional substrate TiO_2/SNFs-GBs-LDPE also exhibited a stable photocatalytic activity after 5 MB degradation experiments (**Figure 2**g).

2.3. Abrasion Tests

Practical applications of superhydrophobic materials are often limited due to the fragility of the nanoscale roughness, which is essential for superhydrophobicity. Often, a soft mechanical impact leads to a substantial decrease in the contact angle or even the total loss of the water-repellence property. Mechanical resistance of the superhydrophobic materials remains one of the major challenges in this field.

Therefore, we further investigated if the micro-meter superstructure does protect the nanoscale SNFs. The 75-µm glass beads (GBs) partially embedded into the LDPE matrix deliver such a superstructure. By changing the GBs concentration in the ethanol suspension, the density of the

GBs on LDPE was controlled. For comparison, we made three different densities of 70, 32, 6.5 units of GBs/mm^2 (**Figure 3**a-c). The cast LDPE substrate was heated to 165°C to be above the glass transition temperature. As a result, GBs sank into the polymer matrix with a certain depth and were fixed in the polymer matrix by cooling down to room temperature. Subsequently, the SNF-coating, TiO_2 NPs synthesis, and hydrophobic treatment are executed as described above (**Figure 3**d-f).

The mechanical abrasion tests were conducted using AB5000 Washability Tester (section 4.2.5). A sponge abrasion head covered with a nitrile glove at a pressure of ca. 1.5 kPa was used in the abrasion test. The abrasion head were moved back and forth on the tested substrate with an effective rubbing distance of 6.5 cm for one direction run. Subsequently, water contact angle of the substrate was measured as a function of the abrasion cycles. In **Figure 3**g, it is shown that the substrates with GB layer have a higher abrasion resistance. The water contact angle decreased by the abrasion cycles. The substrate without GBs showed a fast drop on non-wettability. After 100 cycles, it lost its superhydrophobicity with a CA dropped from 164° to 91°, while the substrates with GBs exhibited higher mechanical durability. It was observed that the substrate GB-32 (with a middle density of GBs cast) produced the best wear resistance, showing a CA of 154° after 100 cycles, on which the superhydrophobicity was maintained. Meanwhile, the GB-70 and GB-6.5 substrates had decreases of CA of about 42° and 50° respectively.

The GBs formed a “mountain-like” microscale roughness, which contributed to the enhanced mechanical durability of the functional substrates. Here, the fragile nanoscale SNFs were well protected by the GBs. The SNFs among the GBs remained stable on the functional substrates after mechanical abrasion compared to the one without casted GBs. A low density of casted GBs on the surface (GB-6.5) leads to weaker hierarchical protection and results in a fast decrease on hydrophobicity. On the other hand, the GB-70 and GB-32 substrates showed a much better abrasion resistance. At higher density, GBs could prevent the SNFs coated on

LDPE surface from the damage of mechanical abrasion. However, GB-70, which has the highest casted GB density, had a higher surface area from the GBs themselves exposed to the abrasion forces. Because of the larger exposure area and the intrinsic hydrophilicity of GBs, the CA of high-density casted substrate GB-70 decreased more than the middle-density cast one GB-32. In **Figure 3**j, the exposure area on the top of GBs was shown according to the abrasion times.

The maintenance of the photocatalytic activity of the substrates was also determined after the abrasion test. The same photo-degradation of MB experiment was conducted, and the relative absorbance was measured before and after the photocatalytic reaction (**Figure 3**h). Corresponding to the CA measurement result, the substrate without GBs protection lost most of the photocatalytic ability among all substrates, following the substrate with low-density cast GBs. The substrates with a high and middle density of casted GBs exhibited similar photocatalytic activity due to the maintenance of the SNFs among the GBs for both substrates, regardless of the density of the GBs. The retained amounts of TiO_2 NPs on SNFs were determined following the same method described in our previous research. Substrates were immersed into a high concentration of sulfuric acid (50%) at 110 °C for 30 min to dissolve all TiO_2 NPs into titanium ion. A calibrated standard line of absorbance to concentration was made using a standard titanium solution in a spectrophotometer. The remaining titanium was a measure for all substrates in **Figure 3**i. The result corresponded with the photocatalytic performance measurement.

2.4. Anti-bacterial Tests

TiO_2 as an antibacterial material has received a lot of attention in the last three decades due to its excellent photocatalytic activity.[34] Researches have discovered the TiO_2 photocatalysts decrease the expression of the genes of bacteria that are involved in the synthesis of signal molecules.[35] Therefore, antibacterial activity is an additional advantage of the as-prepared

functional material due to the induced TiO_2. To compare the anti-bacterial properties, different substrates were used. All LDPE substrate were embedded with GBs before differential treatment. LDPE with bare TiO_2 (TiO_2/GBs-LDPE), LDPE with TiO_2@SNFs coating (TiO_2/SNFs-GBs-LDPE), and LDPE as blank control (GBs-LDPE) were tested with *E. coli* bacterial solution. All vessels used in the tests were sterilized by autoclaving. The substrates were immersed into 10 mL *E. coli* solution and incubated under darkness or 350 nm UV illumination for 90 min (intensity: 6.32 mW/cm^{-2}) at room temperature (**Figure 4**a,d). Next, we followed bacterial cell growth over 210 min at 37°C by measuring absorption at 600 nm (OD_{600}). Five microliters of bacterial solution were taken out after the 90 min incubation and diluted into 50 µL with LB medium and spread on agar plates for overnight growth at 37°C.

The substrates containing TiO_2 after UV illumination exhibited stronger antibacterial activity than those without TiO_2. The *E. coli* concentration decreased after 90 min illumination (**Figure 4**b). Due to more TiO_2 NPs caused by the enlarged surface area of SNFs, the substrate with TiO_2@SNFs showed the strongest antibacterial activity (the concentration of bacteria after 90 min UV illumination was the lowest). The substrates containing TiO_2 without UV illumination or that without TiO_2 (control set) but under UV illumination showed no apparent changes in bacterial inhibition. The growth inhibition shown in **Figure 4**c corresponds with the results shown in **Figure 4**b. Both experiments show that substrates with TiO_2 under UV illumination have an inhibition effect on the growth of *E. coli*. Bacteria were not directly killed by the 350 nm UV radiation, which was consistent with other studies.[36] Wavelengths between 250 and 300 nm are most effective at directly decomposing the cell structure of *E. coli*. The mechanism for killing the bacteria is based on free radicals generated by photoactivated TiO_2 damaging the cell membrane and subsequent leakage of the inner content of *E. coli*. The same phenomenon was observed in other TiO_2 materials,[37] in which Bekboelet et al. used anatase TiO_2 suspension under 300–400 nm irradiation to achieve inactivation of *E. coli* due to the generated hydroxyl radicals. Similarly, Ag/BiOI and C_{70}-TiO_2 composite were used as visible-light-

driven photocatalysts. An obvious reduction of potassium ion (K^+) released from *E. coli* was detected by Fang et al. by using Ag/BiOI composite. [38] Ouyang et al. concluded that using C_{70}-TiO_2 under visible light irradiation created •OH from VB holes oxidization and O_2^{-}• from CB electron transfer, which resulted in a slower propagation of *E. coli*.[39] It was further proof that the radicals generated by photocatalysts targeted on lipids and proteins of *E. coli*.[40]

For a better visual comparison, the colony forming units (CFUs) were counted (**Figure S**7). The bacteria suspensions were collected after the 90-min under UV or darkness, diluted by a factor of 1000, and 5 µL was plated on agar plates for overnight growth at 37°C. The CFUs were determined as shown in **Figure 4**e. The results from the CFU counting were consistent with the OD_{600} trend curves shown previously.

3. Conclusion

In conclusion, we have successfully synthesized a novel multifunctional composite material with superhydrophobicity, photocatalytic ability, and enhanced mechanical durability. The superhydrophobicity has been obtained by the convenient DAGS process (*i.e.,* the reaction of a silane precursor, resulting in an SNFs coating layer with nanoscale roughness observed by SEM). The SNFs exhibited a water contact angle of 168º, non-wettability to various liquids, stability under UV illumination and the self-cleaning effect on solid particles on the surface. TiO_2 NPs were deposited on SNFs, which work as a photocatalyst for the degradation of organic compounds. It was proven that the photocatalytic property was stable by a repeated decomposition of oleic acid and a long-term experiment under daily sun exposure. To protect SNFs from external mechanical damage, GBs (75 µm) were embedded into an LDPE matrix to form a micro/nanoscale hierarchical structure. The performed abrasion test showed a good retainability of superhydrophobic and photocatalytic abilities on the substrates with the hierarchical structure. The GBs density of 32 beads/mm^2 exhibited the best enhancement of durability. We believe that with the improved mechanical resistance and multifunctionalities,

the novel composite material reported here will have a broad range of various applications in both industries and daily life in the future.

4. Experimental Section ((delete section if not applicable))

4.1. Materials

Ethyltrichlorosilane (ETCS, 97%), absolute ethanol and methanol, titanium (IV) fluoride, chloroform (>99.5%), rhodamine 6G, methylene blue (MB), methyl orange, standard titanium solution (1000 µg/mL Ti in H_2O), sulfuric acid (99.8%), and 100 µm-thick low-density polyethylene film were purchased from Sigma-Aldrich and used as received. Glass beads (75 µm diameter) were cleaned with 10% (v/v) aqueous solution of the detergent deconex (Borer Chemie) before use. BL21 *Escherichia Coli* strain was purchased from Life Technologies, Zug, Switzerland, and the pGEX-4T-1 vector from GE Healthcare, Uppsala, Sweden. LB broth was purchased from Carl-Roth AG, Arlesheim, Switzerland, as well as ACS grade ampicillin sodium salt. All solutions were prepared using water treated with a TKA genepure water purification system from TKA Wasseraufbereitungsysteme, Niederelbert, Germany.

4.2. Experiments

4.2.1. Drop cast glass beads on LDPE substrate

A certain weight of 75 µm-diameter GBs was put into 100 mL pure ethanol and under high agitation to form a dispersion. The dispersion went through 20 min ultrasonication at 40°C and was kept under magnetic stirring with a speed of 1000 rpm. Three milliliters of the dispersion was taken out and cast dropwise on a cleaned LDPE substrate with an area of 50 cm^2. After evaporating the ethanol, the substrate was put in an oven at 165°C for 10 min and taken out to cool at room temperature. The GBs were partially embedded into the LDPE matrix, and microscale architecture was formed.

4.2.2. Silicone nanofilaments (SNFs) coating

An oxygen plasma for 5 min at 100 W in a low-pressure plasma generator (Femto, Diener Electronic, Germany) was applied on the LDPE substrate with GBs. The treated substrate was put into a custom-made, 6.5-L gas phase reaction chamber. The relative humidity inside of the chamber was controlled by flushing a mixture stream of dry and wet nitrogen and set to 40% for 1-h equilibrium. The chemical vapor deposition coating was started by injecting 1 mL (7.86 mmol) ethyltrichlorosilane (ETCS) on the centralized stage, made by a watch glass that was placed on a 10-cm high glass stand in the reaction chamber. The gas phase coating was finished after 4 h reaction at 23°C. The substrate coated with SNFs was flushed with nitrogen and stored.

4.2.3. TiO_2 NPs deposition and hydrophobic modification

The SNFs coated substrate was again treated with an oxygen plasma for 5 min at 100 W to become superhydrophilic. After rinsing with deionized water and drying with a nitrogen stream, it was submerged in a 100-mL mixture of ethanol/deionized water (v/v at 4:1). After reaching 60°C, 50 mg (0.4 mmol) of TiF4 was added. The reaction continued for 1.5 h for the depositing of TiO_2 nanoparticles. The substrate was rinsed with deionized water to remove the solvent and hydrochloric acid, further dried at 80°C for 2 h. TiO_2@SNFs@LDPE substrate was made. The hydrophobic modification was conduct according to the same abovementioned method for SNFs coating, while a part of the reaction condition was changed with a relative humidity of 35%, with only 100-μL ETCS injected and a reaction time of 20 min.

4.2.4. Photocatalytic measurements

Methylene blue (MB) degradation was chosen for photocatalytic measurement. A piece of 3 cm × 5 cm TiO_2@SNFs@LDPE substrate was immersed into a quartz beaker which was thermostated at 25°C, with 50 mL MB solution (0.67 ppm MB in methanol: water at 1:1 to wet

the material). An oxygen flow (30 mL/min) was bubbled into MB solution to maintain the oxygen concentration during the photocatalytic reaction. Eight light bulbs (SNE Ultraviolet Co, USA) with emission wavelength at 350 nm were set around the beaker in an RPR-200 model reactor (SNE Ultraviolet Co, USA). Samples (0.3 mL) were taken at defined time intervals, and absorbance was measured by a Perkin-Elmer Lambda 650S UV/vis spectrometer.

4.2.5. Abrasion test

Quantitative measurement was conducted by an abrasion tester (TQC, AB5000) on the modified TiO_2@SNFs@LDPE substrate. A sponge abrasion head was cover with a nitrile glove, with a load of pressure ca. 1.5 kPa. The abrasion head moved back and forth on the tested substrate for a specified time. For each time of movement, the effective rubbing distance is 6.5 cm. After the abrasion test, the substrate was put into a highly concentrated sulfuric acid solution (30% in volume) and heated to 110°C for 30 min to dissolve all TiO_2. The solution was then diluted into 10 times for measurement. The concentration vs. absorbance standard curve was calibrated with a standard solution. The amount loss of TiO_2 scratched off during the abrasion test was measured by a UV-Vis Cary 60 Spectrophotometer (Agilent, USA) at a wavelength of 410 nm by absorbance. The water contact angle change was plotted against the cycle number of the abrasions.

4.2.6. Anti-bacterial test

To confirm the anti-fouling effect of the materials, we used the BL21 *E. coli* strain transformed with the pGEX-4T-1 vector (GE Healthcare), which carries the ampicillin resistance gene. LB (Luria-Bertani) liquid medium supplemented with 100 μg/mL of ampicillin was inoculated with a glycerol stock of bacterial cells, which were cultivated overnight in an orbital shaker at 37°C and 230 rpm. Cell density reached 1.58×10^9 cells/mL based on the optical density at 600 nm (OD_{600}). The cell density was adjusted with same fresh LB to 1.36×10^8 cells/mL (OD_{600} =

0.17). The substrates were immersed into 10 mL *E. coli* solution and incubated under darkness or 350 nm UV illumination for 90 min (intensity: 6.32 mW/cm^{-2}) at room temperature. Next, bacterial growth was followed by measuring the optical density at 600 nm (OD_{600}) over the next 210 min at 37°C to achieve a fast propagation. For the counting of colony forming units (CFUs), the original suspension with bacteria was diluted 1000 times, and 5 µL of the diluted suspension was taken and cast on agar plates for overnight growth (12 h) at 37°C.

4.2.7. Characterization

TEM and EDX analyses were performed on a Tecnai G2 Spirit (FEI, Netherland) at 120 kV. Samples for TEM were scratched off from the slides, ultrasonicated in absolute ethanol for 20 min, dropped onto formvar/carbon film-coated copper grid (Plano GmbH, Germany), and dried in the air for 24 h before use. SEM analysis was done on a Zeiss Supra 50 VP (Zeiss, Germany) at 10 kV using the mixed detector of in-lens and SE2. Before use, 8-nm platinum was sputtered on the sample by a CCU-010 HV coating unit (Safematic, Switzerland). The water contact angle and sliding angle measurements were performed on the respective surfaces with a Drop Shape Analyzer (DSA100) (Kruss, Germany). At least five different positions were measured on each substrate surface.

Supporting Information

Supporting Information is available from the Wiley Online Library or from the author.

Acknowledgements

The authors are grateful to Swiss National Fund and Alfred-Werner-Legat for financial support. The authors thank the centre of microscopy and image analysis of the University of Zurich for providing their facilities. They also thank Valentin Dubois for the scheme drawing.

Received: ((will be filled in by the editorial staff))
Revised: ((will be filled in by the editorial staff))
Published online: ((will be filled in by the editorial staff))

References

[1] R. E. Johnson, R. H. Dettre, *Journal of Physical Chemistry* **1964**, *68*, 1744-&.

[2] X. F. Gao, L. Jiang, *Nature* **2004**, *432*, 36-36.

[3] G. M. Zhang, J. Zhang, G. Y. Xie, Z. F. Liu, H. B. Shao, *Small* **2006**, *2*, 1440-1443.

[4] a) V. A. Ganesh, H. K. Raut, A. S. Nair, S. Ramakrishna, *Journal of Materials Chemistry* **2011**, *21*, 16304-16322; b) I. P. Parkin, R. G. Palgrave, *Journal of Materials Chemistry* **2005**, *15*, 1689-1695.

[5] P. Ragesh, V. A. Ganesh, S. V. Naira, A. S. Nair, *Journal of Materials Chemistry A* **2014**, *2*, 14773-14797.

[6] A. Fujishima, T. N. Rao, D. A. Tryk, *Electrochimica Acta* **2000**, *45*, 4683-4690.

[7] a) M. H. Jin, X. J. Feng, J. M. Xi, J. Zhai, K. W. Cho, L. Feng, L. Jiang, *Macromolecular Rapid Communications* **2005**, *26*, 1805-1809; b) A. Lafuma, D. Quéré, *Nature Materials* **2003**, *2*, 457; c) T. Onda, S. Shibuichi, N. Satoh, K. Tsujii, *Langmuir* **1996**, *12*, 2125-2127.

[8] W. Barthlott, C. Neinhuis, *Planta* **1997**, *202*, 1-8.

[9] a) Z. L. Chu, S. Seeger, *Chemical Society Reviews* **2014**, *43*, 2784-2798; b) X. Zhang, F. Shi, J. Niu, Y. Jiang, Z. Wang, *Journal of Materials Chemistry* **2008**, *18*, 621-633; c) A. Nakajima, *Npg Asia Materials* **2011**, *3*, 49.

[10] C. R. Crick, S. Ismail, J. Pratten, I. P. Parkin, *Thin Solid Films* **2011**, *519*, 3722-3727.

[11] X. Chen, S. S. Mao, *Chemical Reviews* **2007**, *107*, 2891-2959.

[12] a) Z. He, M. Ma, X. Lan, F. Chen, K. Wang, H. Deng, Q. Zhang, Q. Fu, *Soft Matter* **2011**, *7*, 6435-6443; b) D. Goswami, S. K. Medda, G. De, *ACS Applied Materials & Interfaces* **2011**, *3*, 3440-3447.

[13] G. B. Hwang, K. Page, A. Patir, S. P. Nair, E. Allan, I. P. Parkin, *ACS Nano* **2018**, *12*, 6050-6058.

[14] A. Fujishima, K. Honda, *Nature* **1972**, *238*, 37.

[15] a) S. Nahar, M. F. M. Zain, A. A. H. Kadhum, H. A. Hasan, M. R. Hasan, *Materials* **2017**, *10*, 629; b) J. Low, B. Cheng, J. Yu, *Applied Surface Science* **2017**, *392*, 658-686; c) M. Ratova, P. J. Kelly, G. T. West, *Materials Chemistry and Physics* **2017**, *190*, 108-113.

[16] V. Bolis, C. Busco, M. Ciarletta, C. Distasi, J. Erriquez, I. Fenoglio, S. Livraghi, S. Morel, *Journal of Colloid and Interface Science* **2012**, *369*, 28-39.

[17] T. Adachi, S. S. Latthe, S. W. Gosavi, N. Roy, N. Suzuki, H. Ikari, K. Kato, K.-i. Katsumata, K. Nakata, M. Furudate, T. Inoue, T. Kondo, M. Yuasa, A. Fujishima, C. Terashima, *Applied Surface Science* **2018**, *458*, 917-923.

[18] T. Kamegawa, Y. Shimizu, H. Yamashita, *Adv Mater* **2012**, *24*, 3697-3700.

[19] a) J. Z. Zimmermann, CH), Seeger, Stefan (Zumikon, CH), Artus, Georg (Birmensdorf, CH), Jung, Stefan (Kilchberg, CH), UNIVERSITY OF ZURICH (Office Vice President of Research, Ramistrasse 71, Zurich, CH), United States, **2007**; b) G. Artus, J. Zimmermann, S. Seeger, S. Jung, **2003**.

[20] a) J. Zimmermann, M. Rabe, D. Verdes, S. Seeger, *Langmuir* **2008**, *24*, 1053-1057; b) J. Zimmermann, M. Rabe, G. R. J. Artus, S. Seeger, *Soft Matter* **2008**, *4*, 450-452; c) B. C. Li, L. Wu, L. X. Li, S. Seeger, J. P. Zhang, A. Q. Wang, *Acs Applied Materials & Interfaces* **2014**, *6*, 11581-11588.

[21] a) J. Zimmermann, F. A. Reifler, G. Fortunato, L. C. Gerhardt, S. Seeger, *Advanced Functional Materials* **2008**, *18*, 3662-3669; b) Z. L. Chu, S. Seeger, *Rsc Advances* **2015**, *5*, 21999-22004.

[22] D. M Cox, *High Surface Area Materials*, **1999**.

[23] A. B. D. Cassie, S. Baxter, *Transactions of the Faraday Society* **1944**, *40*, 0546-0550.

[24] a) T. Yanagisawa, A. Nakajima, M. Sakai, Y. Kameshima, K. Okada, *Materials Science and Engineering: B* **2009**, *161*, 36-39; b) Y. C. Jung, B. Bhushan, *ACS Nano* **2009**, *3*, 4155-4163; c) J. Zhang, S. Seeger, *ChemPhysChem* **2013**, *14*, 1646-1651.

[25] a) H. Zhou, H. Wang, H. Niu, A. Gestos, T. Lin, *Advanced Functional Materials* **2012**, *23*, 1664-1670; b) Z. L. Chu, S. Seeger, *Advanced Materials* **2015**, *27*, 7775-7781.

[26] G. R. J. Artus, S. Olveira, D. Patra, S. Seeger, in *Macromolecular Rapid Communications, Vol. 38*, **2017**.
[27] G. R. Meseck, R. Kontic, G. R. Patzke, S. Seeger, *Advanced Functional Materials* **2012**, *22*, 4433-4438.
[28] M. Eslamian, F. Zabihi, *Nanoscale Research Letters* **2015**, *10*.
[29] S. Q. Liu, A. Pandey, J. Duvigneau, J. Vancso, J. H. Snoeijer, *Macromolecules* **2018**, *51*, 2411-2417.
[30] G. R. J. Artus, S. Jung, J. Zimmermann, H. P. Gautschi, K. Marquardt, S. Seeger, *Advanced Materials* **2006**, *18*, 2758-+.
[31] a) J. Zimmermann, F. A. Reifler, U. Schrade, G. R. J. Artus, S. Seeger, *Colloids and Surfaces a-Physicochemical and Engineering Aspects* **2007**, *302*, 234-240; b) G. R. J. Artus, S. Seeger, *Advances in Colloid and Interface Science* **2014**, *209*, 144-162.
[32] a) J. Schneider, M. Matsuoka, M. Takeuchi, J. Zhang, Y. Horiuchi, M. Anpo, D. W Bahnemann, *Understanding TiO2 Photocatalysis: Mechanisms and Materials, Vol. 114*, **2014**; b) A. L. Linsebigler, G. Lu, J. T. Yates, *Chem. Rev.* **1995**, *95*, 735-758.
[33] G. R. Meseck, A. Kach, S. Seeger, *Journal of Physical Chemistry C* **2014**, *118*, 24967-24975.
[34] a) J. Prakash, S. Sun, H. C. Swart, R. K. Gupta, *Applied Materials Today* **2018**, *11*, 82-135; b) R. A Damodar, S.-J. You, H.-H. Chou, *Study the self cleaning, antibacterial and photocatalytic properties of TiO2 entrapped PVDF membranes, Vol. 172*, **2009**.
[35] A. Kubacka, M. Suarez-Diez, D. Rojo, R. Bargiela, S. Ciordia, I. Zapico, J. Albar, C. Barbas, V. Martins dos Santos, M. Fernández-García, M. Ferrer, *Understanding the antimicrobial mechanism of TiO2-based nanocomposite films in a pathogenic bacterium, Vol. 4*, **2014**.
[36] N. Vermeulen, W. J. Keeler, K. Nandakumar, K. T. Leung, *Biotechnology and Bioengineering* **2008**, *99*, 550-556.
[37] M. Bekbolet, C. V. Araz, *Chemosphere* **1996**, *32*, 959-965.
[38] Z. K. Fang, J. N. Yang, Y. Cao, L. F. Zhu, Q. Zhang, D. Shu, C. He, *2013 International Symposium on Environmental Science and Technology (2013 Isest)* **2013**, *18*, 503-508.
[39] K. Ouyang, K. Dai, S. L. Walker, Q. Huang, X. Yin, P. Cai, *Scientific Reports* **2016**, *6*, 25702.
[40] G. Carre, E. Hamon, S. Ennahar, M. Estner, M. C. Lett, P. Horvatovich, J. P. Gies, V. Keller, N. Keller, P. Andre, *Applied and Environmental Microbiology* **2014**, *80*, 2573-2581.

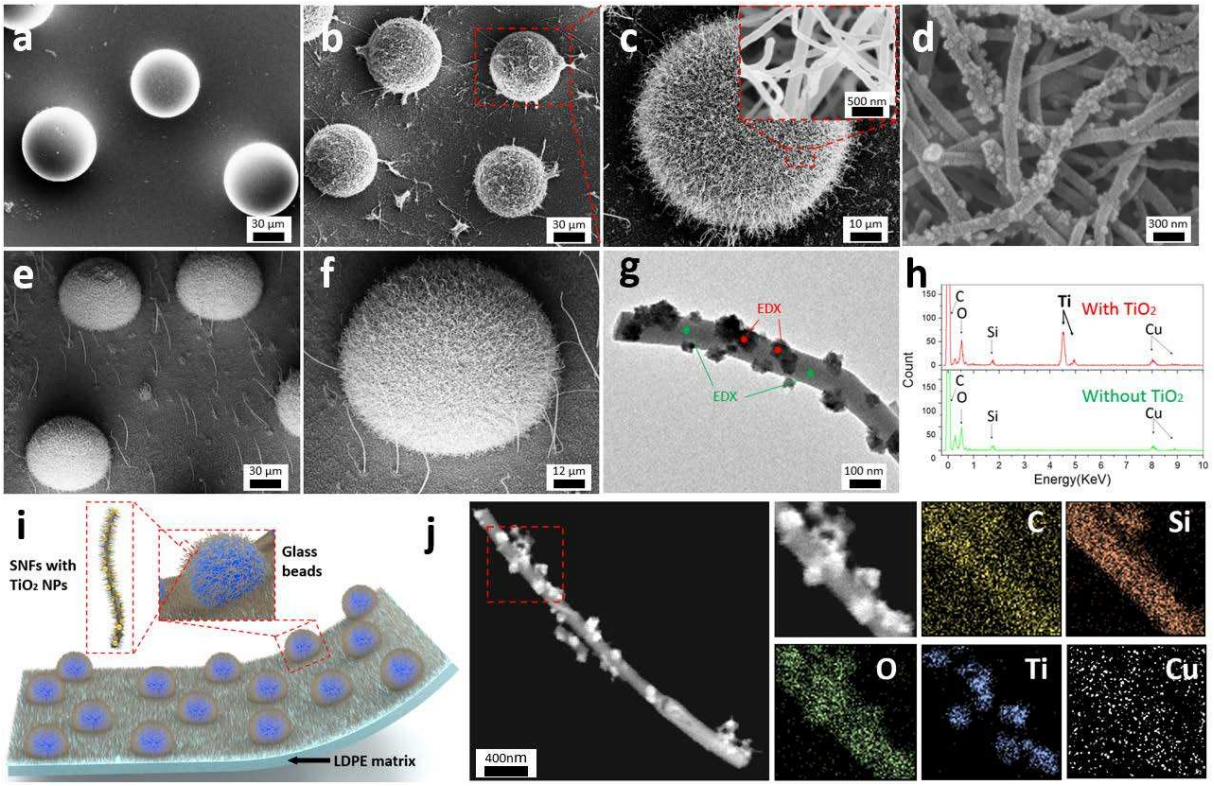

Figure 1. Characterization of the functional substrate. (a-f) SEM images of (a) step 1, LDPE matrix with GBs; (b,c) step 2, LDPE with GBs matrix coated with SNFs; (d) step3, functionalized SNFs with TiO_2 NPs; and (e,f) side view of the functional substrates with an observation angle of 65° . (g) A TEM image of (f) SNFs with TiO_2 NPs and (h) EDX spectra corresponding to (g). (i) Illustrative graph of the functional substrates. (j) STEM EDX mapping of SNFs with TiO_2 NPs according to elements.

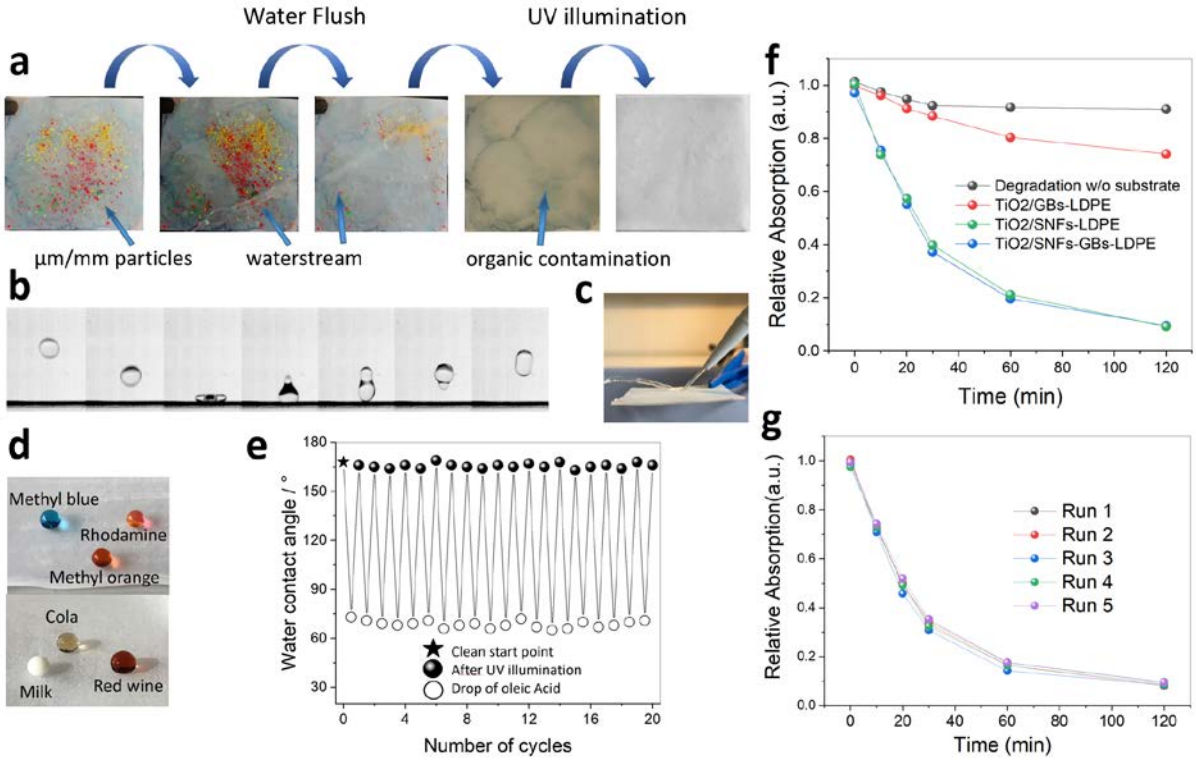

Figure 2. Self-cleaning properties of the functional substrate. (a) Image of the anti-fouling process. The substrate was contaminated by ground chalk particles and drop casted methylene blue ethanol solution. (b,c) Water repellence effect captured by b) high-speed camera and c) normal camera. (d) The non-wettability of various liquids on the substrates. (e) The recyclability of the substrate characterized by the contact angle after contaminated by oleic acid and UV illumination for 20 cycles. (f) The photodegradation of methylene blue (MB) solution (1 ppm MB in 1:1 methanol-water mixture to wet the hydrophobic surface) in the presence of functional substrate with one side area of 6 cm^2 under UV irradiation at 350 nm in the first graph (blank = degradation of MB without any substrate; red = degradation with TiO_2-GBs-LDPE; green = degradation with TiO_2/SNFs-LDPE; blue = degradation with TiO_2/SNFs-GBs-LDPE). (g) The recycling experiment of the degradation of MB with TiO_2/SNFs-GBs-LDPE for five runs.

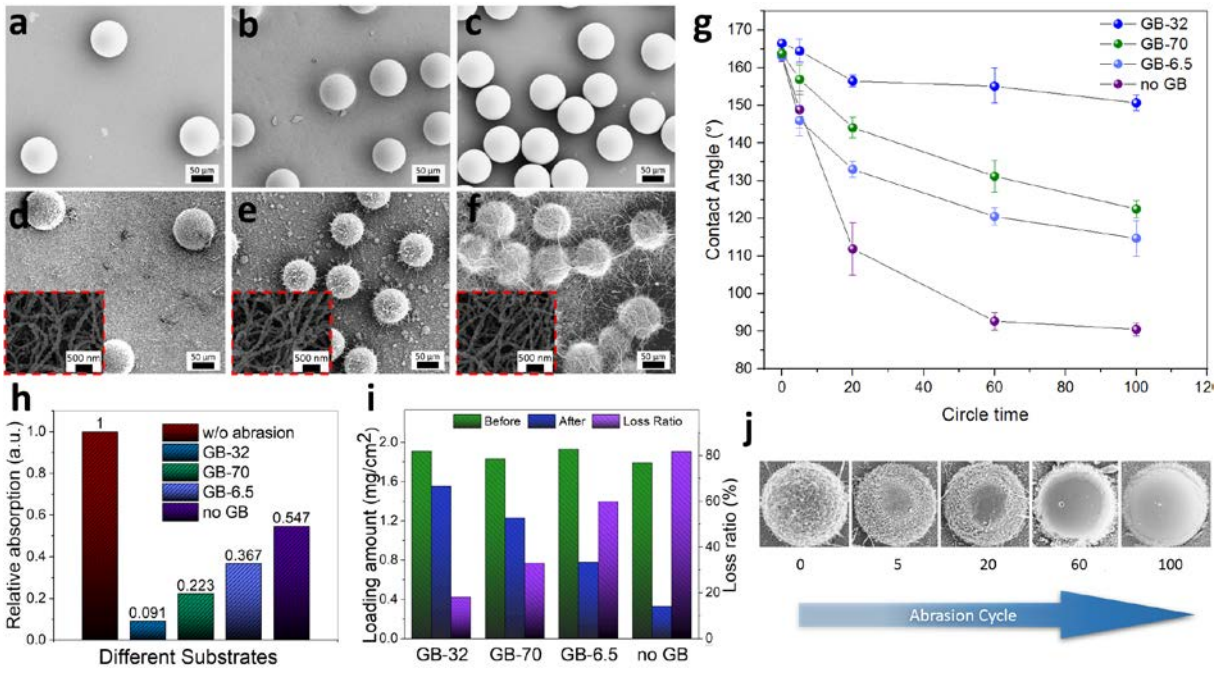

Figure 3. Abrasion tests. SEM images: (a-c) GBs drop cast LDPE templates with different density of 6.5, 32, 70 units of GBs/mm^2; (d-f) Functional substrates of these three densities of GBs (LDPE templates further coated with SNFs, deposited with TiO_2 NPs and hydrophobic modification). (g) Contact angle change trend of functional substrates according to abrasion cycle time. (h) The photocatalytic performance of 2-h MB degradation by different substrates after 100 cycles of abrasion. (i) The loading amount of TiO_2 NPs on different substrates before and after 100 cycles of abrasion. (j) SEM images of GBs with incremental abrasion cycles.

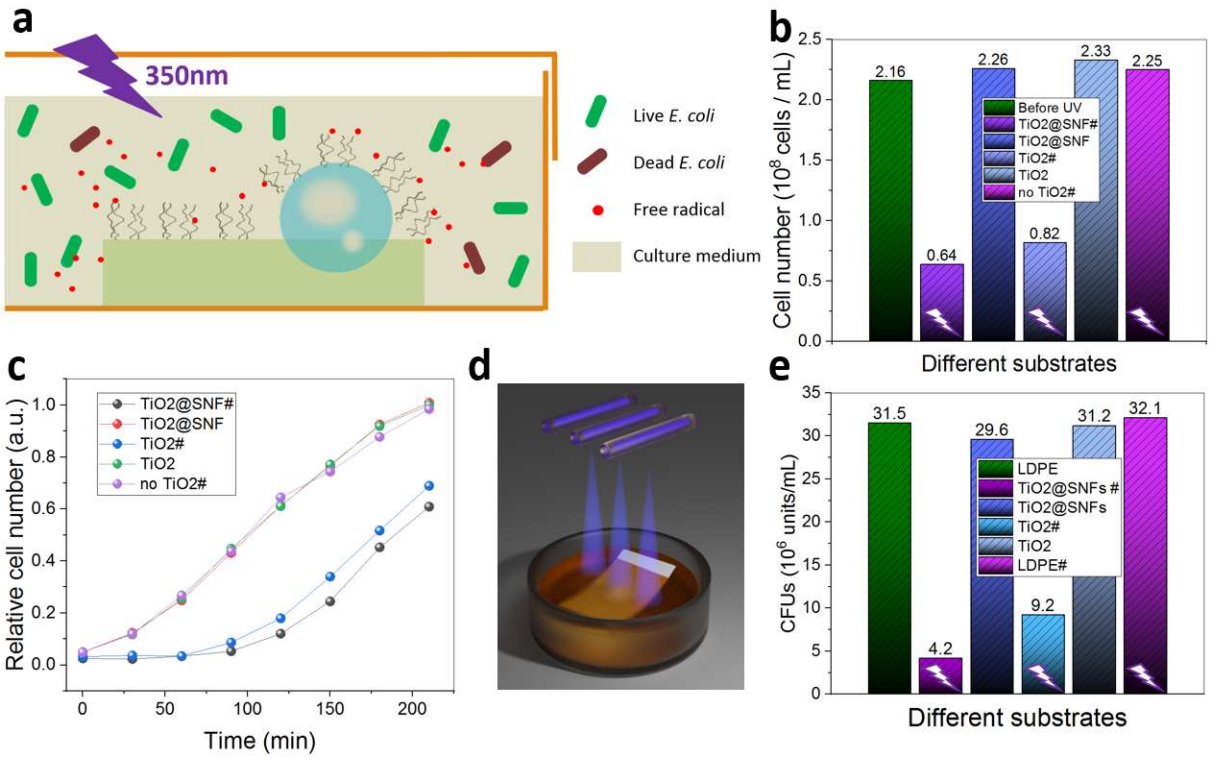

Figure 4. (a) Schematic illustration of the anti-bacterial experiment. (b) The cell concentration of solutions with different substrates after 90 min under darkness or UV illumination at room temperature. (c) The bacterial growth curve (OD_{600}) after 90 min of darkness or UV illumination. (d) Illustrative graph of a sample exposed under UV illumination. (e)The colony forming units (CFUs) resulted from incubation of *E. coli* in agar plates for 12 h at 37 °C. The initial solution was taken from the solutions after 90 min under darkness or UV illumination cultivation. # represents the UV illumination.

Keyword
self-cleaning, superhydrophobic, photocatalytic, hierarchical structure, mechanical durable